

Research Article

Yoann Brûlé*, Peter Wiecha, Aurélien Cuche, Vincent Paillard, and Gérard Colas des Francs

Magnetic and electric Purcell factor control through geometry optimization of high index dielectric nanostructures

Abstract: We use evolutionary algorithms coupled to the Green's Dyadic Method (GDM) in order to optimize the geometry of planar dielectric nanoantennas designed for controlling the emission rate of magnetic or electric dipolar emitters (so-called Purcell factor). Depending on the nature and orientation of the dipoles, different optimized shapes are obtained, all presenting regular and periodical features. We discuss the physical origin of the obtained designs. GDM relies on spatial meshing well adapted to optimize nanostructures of finite thickness nanofabricated by e-beam lithography. However, optimized structures present morphological resonances extremely sensitive to the object shape. Therefore, we complete our study considering finite element method to determine the maximum achievable magnetic Purcell factor. We assume the shape obtained from evolutionary optimization and determine the dimensions of a feasible 100 nm thickness planar dielectric silicon nanoantenna deposited on a glass substrate that leads to a $\simeq 2 \times 10^3$ enhancement of the spontaneous decay rate of the magnetic dipolar transition in Eu^{3+} ions. This work paves the way toward innovative applications of magnetic light-matter interactions such as optical negative-index metamaterials or quantum technological components.

Keywords: Purcell effect, Evolutionary optimization, High-index dielectric, Periodic nanostructures

1 Introduction

The coupling of the magnetic part of light to atoms is much weaker than the electric one. Indeed, magnetic dipole transitions are α^2 weaker than electric dipole transitions, where $\alpha \simeq 1/137$ is the fine-structure constant [1]. Hence, the development of novel applications based on magnetic response in the optical regime, such as negative-index metamaterials [2] or efficient nanoantennas [3], requires to focus on the engineering of the magnetic Local Density Of States (LDOS) in order to enhance the magnetic contribution to light matter interaction. As predicted by E. M. Purcell more than 70 years ago for "nuclear magnetic moment at radio frequencies", the interaction of light and especially the spontaneous emission rate of solid state emitter can be drastically enhanced by its surrounding photonics environment which is well-known as the *Purcell effect* [4]. In other words, by placing a dipolar emitter into an optical micro-cavity or near a resonant nanostructure, it is possible to drastically modify its emission rate. Until recently, those interactions were mainly focused on plasmonics, as noble metals nanostructures support Localized Surface Plasmon Resonances (LSPR) that are tunable by size, shape and constituent materials [5–7]. However, despite impressive advances, severe limitations on the use of metals, such a high dissipation losses and poor compatibility with Complementary Metal Oxide Semiconductor (CMOS) technology, prevent them to be used in integrated devices. In order to overcome those limitations, replacing plasmonic resonators by high refractive index dielectric ones such as Silicon (Si) becomes interesting [8]. As the Si refractive index is above 3.5 and is associated to a very

*Corresponding author: Yoann Brûlé, Gérard Colas des Francs, ICB, Université de Bourgogne-Franche Comté, CNRS, Dijon, France, e-mail: yoann.brule@u-bourgogne.fr, gerard.colas-des-francs@u-bourgogne.fr

Peter Wiecha, LAAS, Université de Toulouse, CNRS, Toulouse, France, e-mail: pwiecha@laas.fr

Aurélien Cuche, Vincent Paillard, CEMES-CNRS, Université de Toulouse, CNRS, Toulouse, France, e-mail: aurelien.cuche@cemes.fr, vincent.paillard@cemes.fr

low extinction coefficient below its direct bandgap [9], it allows to obtain Mie resonances in the visible to the near-infrared domain using Si nanostructures with sub-wavelength dimensions. Moreover, the high index dielectric contrast between the Si nanostructure and its low index environment (*e.g.* $n \simeq 1.5$ for silica) ensures a high confinement and near field intensity. The use of Si also guarantees a fully compatible CMOS technology for fabrication with large scalability and perfect reproductibility [8, 10–12]. Regarding the quantum emitters, rare-earth ions such as Europium ions (Eu^{3+}) are particularly relevant as they exhibit efficient electric and magnetic transitions in the visible domain [13–19]. Moreover, synthesis of rare earth sesquioxides (Y_2O_3 , Gd_2O_3) thin films doped with such luminescent elements has become accessible [17] allowing to investigate the design of planar high index dielectric cavities coupled to such kind of emitters. In this context, numerical optimization is a particularly relevant tool. Since few decades, it has been largely applied to various domains of nanophotonics. While first attempts were focusing on the inverse design of optical coatings and multilayered structures [20, 21], development of efficient algorithms associated to numerous flexible computational tools and improvement in computational power [22], have allowed the design of various optical components with desired properties [23] such as plasmonic [24–27] or dielectric [10, 28] nanoantennas, compact broadband on-chip wavelength demultiplexer [29] or plasmonic and dielectric metasurfaces [30]. To do so, various class of algorithms have been used such as gradient-based methods [31], Evolutionary Optimization (EO) techniques [32] and more recently deep learning approaches [33–36]. In this article, we apply a subset of EO algorithms called Differential Evolution (DE) [37] in order to optimize the geometrical design of planar Si dielectric structures coupled to Gd_2O_3 thin film doped with Eu^{3+} emitters for maximizing or minimizing the decay rate enhancements (*i.e.* the Purcell factor) of magnetic and electric dipolar transitions that occur in Eu^{3+} at wavelengths of $\lambda_m = 590$ nm and $\lambda_e = 610$ nm, respectively. In order to discuss the physical origin of the retrieved designs, we then use another approach based on the work developed by Mignuzzi *et al.* in [38].

2 Green Dyadic Method and differential evolution algorithm applied to geometrical photonic optimization

Magnetic and electric Purcell factors characterize the decay rate enhancement of magnetic (MD) and electric dipolar (ED) transitions, respectively. In this work, the emitters are europium ions doping Gd_2O_3 matrix since they present both ED and MD transitions [13–19]. We investigate the enhancement of their emission by coupling them to silicon nanostructures of arbitrary shape but same thickness 100 nm. Purcell factor is proportional to the local density of states (LDOS). We have used the Green Dyadic Method (GDM) [39] and especially the python toolkit pyGDM [40, 41]. It allows to perform decay-rate calculation inside multi-material nanostructures through a formalism based on field-susceptibilities for the derivation of the LDOS [26, 40, 42, 43]. The GDM is based on a volumic discretization of the nanostructures. In order to limit computational resources and consider realistic shapes, the cubic mesh size has been limited to 20 nm, slightly above the resolution of standard e-beam lithography. It is worth mentioning that comparison with Mie analytical model has demonstrated that the decay is strongly sensitive to the meshing [41]. We attribute this mainly to the strong sensitivity of morphological resonances with respect to the object shape. For the current work we estimate the error of the order of 5% for the electric Purcell factor but up to 30-50% for magnetic Purcell factor. Since we will observe that the arbitrarily optimized structures also rely on resonances, we will complete this study in a second step, considering finite element method, better adapted to described rounded object.

EO algorithms are inspired from the evolution theory [32]. These bio-inspired algorithms can be classified as stochastic ones as they iteratively use random mutations of an initial random population of candidates in order to make it evolves towards one population whose individuals present the best predefined characteristics. These characteristics can be implemented by one (single objective [44]) or several (multi-objective [10, 45]) fitness functions to maximize (or minimize). To converge, these algorithms apply the following process.

The fitness functions of each individual of the current generation is evaluated. A mutation and a crossover is performed to form trial individuals. The trial individuals fitness functions are then re-evaluated and a selection is operated in order to form a new generation with better characteristics. The process is then repeated iteratively (see Fig. 1). These algorithms aim to find the global optimal solution of problems with large and complex dimensionality. They can indeed be seen as global optimization techniques. It has been recently applied to the better understanding of natural design of photonic architectures that has been optimized through natural evolution [46]. While trying to retrieve the peculiar architecture of the *Morpho rhetenor* butterfly iridescent blue wings scale [47], Barry *et al.* have been able to make these algorithms converge toward this regular and interdigitated periodic photonic nanostructures through the definition of a suitable fitness function (minimize the specular reflection at any given wavelength, and maximize the scattering of blue light in the higher diffraction orders) associated to relevant constraints (structure as light as possible) [46]. Regarding the optimization of nanoantennas geometry, EO algorithms have been applied to maximize the near field intensity or the Purcell effect in dielectric nanostructures in [28, 48] and in plasmonic ones in [24–26]. It is worth noticing that regular and/or periodic patterns appear in the optimization performed in [26, 48].

In the following, we are presenting the results obtained by applying a specific type of EO algorithms, Differential Evolution [37] (whose simplified cycle is recalled in the Fig. 1), and its self adaptive "jDE" implementation for single objective problem [44] available in the Python "pyGMO" interface associated to the "paGMO" library [49] and to the Python toolkit pyGDM [40, 41] in order to optimize either the electric or magnetic Purcell effect in Eu^{3+} doped Gd_2O_3 matrix of refractive index $n_1 = 1.8$ through the nanostructuring of a planar 100 nm Si environment deposited on a SiO_2 substrate $n_2 = 1.5$. Refractive index of the silicon n_{Si} has been taken from [50]. The coupling between EO and the pyGDM numerical simulations can be found in [10]. We are using the default "/rand/1/exp" parameter for the mutation variant of the jDE algorithm and its default configuration for the auto-adaptation scheme.

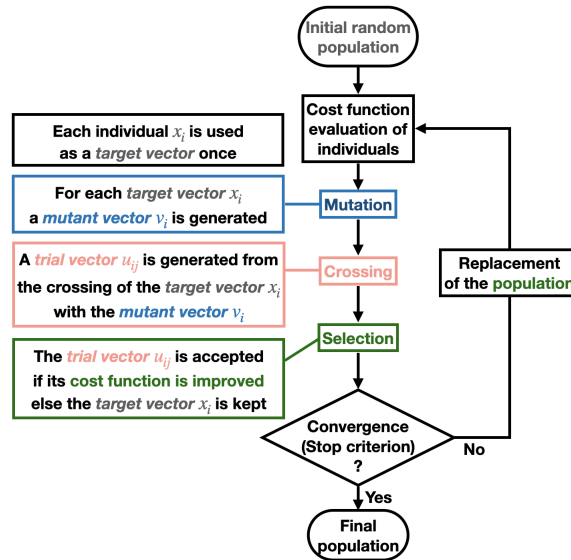


Fig. 1: Algorithm of the differential evolution cycle for topological optimization

The core emitter (Gd_2O_3 doped with Eu^{3+}) consists in a nanocylinder of 100 nm height and 50 nm diameter. In reality, this Gd_2O_3 -doped cylinder would contain a lot of emitters with arbitrary orientation. The emission characteristics of this real configuration could be optimized but for a sake of simplicity and understanding, we have limited the study to single emitter with defined orientation. Thus, we have fixed

the optimization goal to find the Si nanostructure that maximizes or minimizes the magnetic (*resp.* electric) decay rate enhancement Γ_m/Γ_0 (*resp.* Γ_e/Γ_0) at wavelength of λ_m (*resp.* λ_e) for an emitter situated at the center of the core $\mathbf{r}_0 = [0, 0, 50]$ nm and oriented either along or perpendicular to the substrate. Hence, we are optimizing the planar nanostructured Si environment which is constituted of $N = 300, 400, 500,$ and 600 Si nanopillars (each $20 \text{ nm} \times 20 \text{ nm} \times 100 \text{ nm}$) lying on a SiO_2 substrate in an area limited to $1.68 \times 1.68 \mu\text{m}^2$. The surrounding medium is air. A population of 64 individuals is evolving. Each of which is a set of (x, y) positions chosen among a $20 \times 20 \text{ nm}^2$ discretized grid of the $1.68 \times 1.68 \mu\text{m}^2$ plane, core emitter positions excluded (*i.e.* $85^2 - 5 = 7220$ possible positions). The next section presents the results of the optimization for the magnetic (*resp.* electric) dipolar emissions. For the sake of clarity, we discuss in the main text two representative configurations, leading to the highest Purcell factor: namely out of plane MD and in-plane ED. The others configurations lead to similar designs and are presented in the supplementary materials.

3 Geometrical optimizations

3.1 Optimization of the Purcell factor for an out of plane MD

3.1.1 Maximization (Enhancement of the decay rate)

In Fig. 2, we present the results of the optimization for the decay rate enhancement of the magnetic dipolar emission of Eu^{3+} at $\lambda_m = 590 \text{ nm}$ and for a dipole polarized along the z -axis (perpendicularly to the substrate). We only show the results of the optimization for $N = 400$ Si blocks. Numerical simulations were repeatedly reproduced with different numbers of Si blocks and all leads to similar shapes as well as optimized Purcell factors (see supplementary materials).

The optimization has been stopped after $N_{it} = 8390$ iterations with $N_{imp} = 1485$ improvements of the

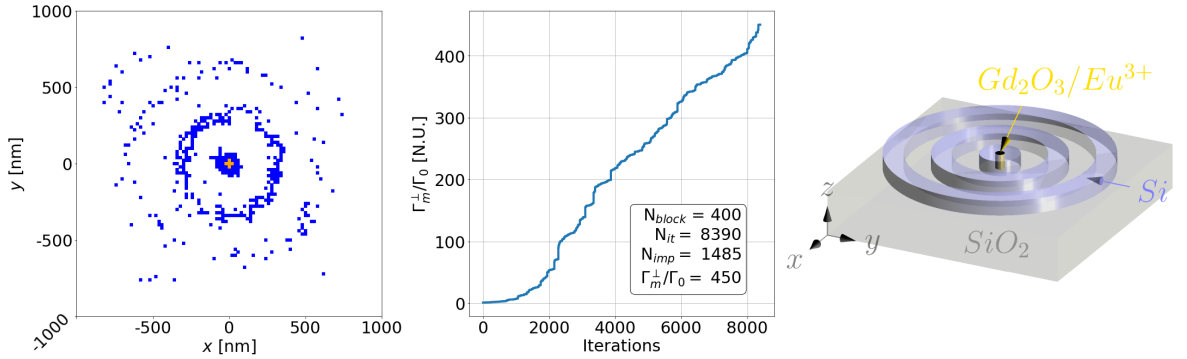


Fig. 2: Left : XY -plane projection of the optimized structure (orange : fixed core emitter, blue : Si nanopillars), Center : Evolution of the magnetic Purcell factor Γ_m^\perp/Γ_0 through the optimization iterations, Right : Scheme of the found nanostructure.

fitness function (Γ_m^\perp/Γ_0) of the best candidate among the full 64 individuals of the population. It converges towards a regular structure that consists in a Si shell of diameter $\simeq 200 \text{ nm}$ surrounding the $\text{Gd}_2\text{O}_3/\text{Eu}^{3+}$ doped core and concentric Si rings of width $\simeq 100 \text{ nm}$ and period $\simeq 300 \text{ nm}$. The associated enhancement of the magnetic decay rate is evaluated to $\Gamma_m^\perp/\Gamma_0 = 450$. We can also notice another concentric nanoring emerging at the border of the optimization area which should be increased to make it fully appear. We can presume that an optimization on a larger area with more Si blocks would converge toward a cylindrical grating.

3.1.2 Minimization (Inhibition of the decay rate)

Reversely, we can minimize the MD transition at $\lambda_e = 590$ nm, see Fig. 3. It converges towards a regular structure that consists in concentric Si rings of width $\simeq 80$ nm and period $\simeq 250$ nm without shell around the core emitter. The associated inhibition of the magnetic decay rate is evaluated at approximately $\Gamma_0/\Gamma_m^\perp \simeq 6.5$. We can observe that the optimized structure for the inhibition is complementary to the one of the exaltation.

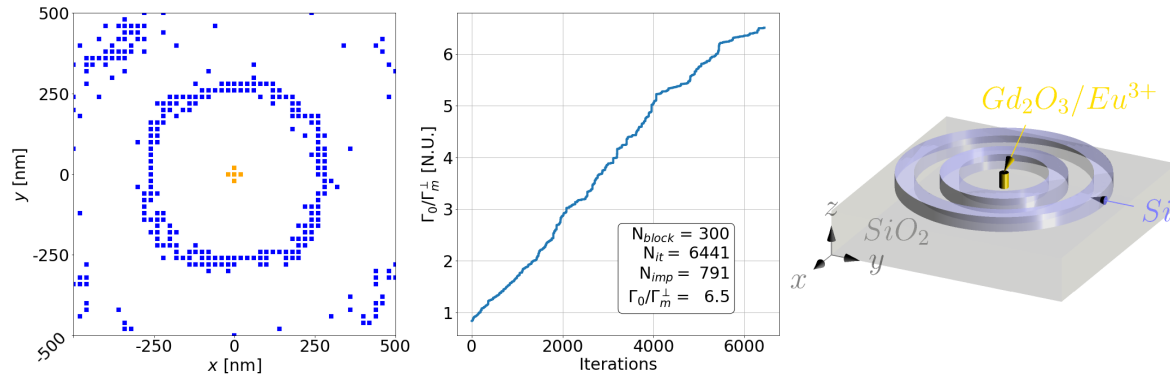


Fig. 3: Left : XY -plane projection of the optimized structure (orange : fixed core emitter, blue : Si nanopillars), Center : Evolution of the magnetic decay rate inhibition Γ_0/Γ_m^\perp through the optimization iterations, Right : Scheme of the found nanostructure. The area of optimization is limited to a 500×500 nm² plane and the number of block is $N = 300$.

3.2 Optimization of the Purcell factor for an in-plane ED

For comparison purpose, we present in Fig. 4 the optimization of the in plane electric Purcell factor (for an electric dipolar emission of Eu^{3+} at $\lambda_e = 610$ nm and oriented along the x -axis), considering $N = 300$ Si blocks. The optimized structure leads to an in-plane electric Purcell factor $\Gamma_e^\parallel/\Gamma_0 \simeq 125$.

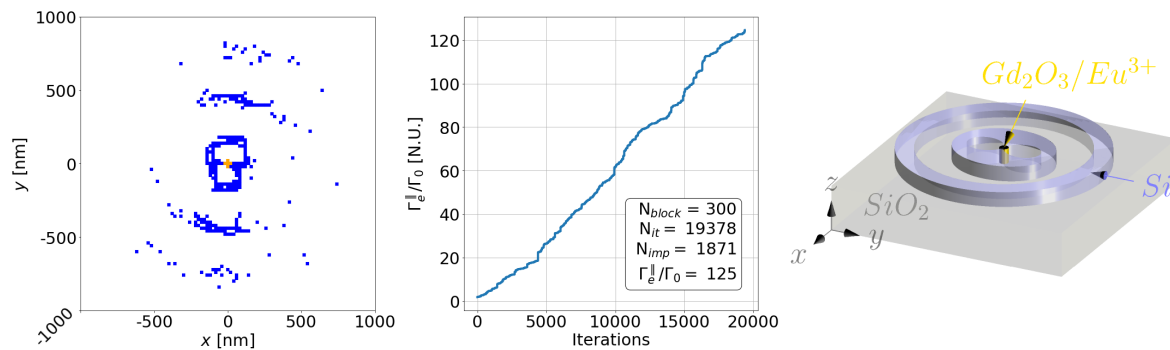


Fig. 4: Left : XY -plane projection of the optimized structure (orange : fixed core emitter, blue : Si nanopillars), Right : Scheme of the found nanostructure.

Regularity is emerging one more time. A bowtie antenna perpendicular to the ED oscillation is formed and circular rings also appear (see Fig. 4). Additional simulations with different numbers of Si blocks lead to similar results. Figure 5 present the superposition of the structures obtained optimizing with $N = 300, 400,$

500 and 600 Si nanopillars and clearly reveals that all optimized structures present similar features, namely a bowtie antenna and circular rings.

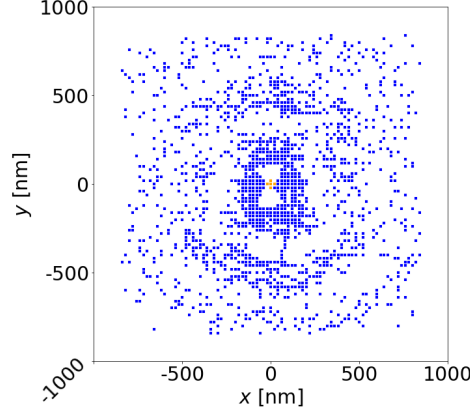


Fig. 5: XY -plane projection of the structure arising from the superposition of four independent EO evolving $N = 300, 400, 500$ or 600 Si blocks (orange : fixed core emitter, blue : Si nanopillars).

3.3 Discussion

To summarize, apart from the presence of a Si core that depends on both the dipole nature and orientation, we observe similar bullseye like nanostructures [51] for all the configurations. The circular concentric rings act as planar cylindrical Bragg mirror and define a planar cavity that strongly enhance the dipolar emission. As far as the near-field zone is concerned, we observe strong differences for ED and MD emitters. In case of in-plane ED, a complex bowtie shaped nanoantenna, of which tips are oriented along the ED axis, is retrieved. This bowtie shape reminds notably the nanostructures obtained in [38, 48, 55]. In ref. [48], an EO algorithm was applied to an analog situation, that is improving the confinement of an in plane electric field. Hence similar optimized design is retrieved since the Purcell factor is inversely proportional to the mode volume. Differently, in ref. [55] the authors introduced the concept of mode matching to optimize the coupling of an electric emitter to a plasmonic nanoantenna but obtained similar features, revealing the generality of the achieved configurations. In case of MD, we observe a nanodisk that surrounds directly the emitters. Such geometry has already been identified as good candidates for maximizing the magnetic Purcell factor [53, 54], but this clearly reveals that it is close to optimal.

We use the approach of Mignuzzi and coworkers on the "nanoscale design of the LDOS" [38] to access physical understanding of the achieved optimized structures. To this purpose, they have derived a volume integral for the expression of the decay rate enhancement so that they can assess *locally* the effect of matter on the electric decay rate, namely enhancement or inhibition. This reveals where to remove materials to strengthen the enhancement effect solely. Let us summarize their derivation before considering the magnetic case. The decay rate associated to an electric dipole \mathbf{d} is expressed as

$$\frac{\Gamma_e}{\Gamma_0} = 1 + \frac{6\pi\epsilon_0}{k_0^3 |d|^2} \text{Im} \{ \mathbf{d} \cdot \mathbf{E}_s(\mathbf{r}_d) \} \quad (1)$$

where $\mathbf{E}_s(\mathbf{r}_0)$ is the dipolar electric field scattered at the position of the dipole in its complex surroundings. In addition, the reciprocity theorem states that for current source density \mathbf{J}_0

$$\int d^3\mathbf{r} \mathbf{J}_0(\mathbf{r}) \cdot \mathbf{E}_s(\mathbf{r}) = \int d^3\mathbf{r} \mathbf{J}_s(\mathbf{r}) \cdot \mathbf{E}_0(\mathbf{r}) \quad (2)$$

where $\mathbf{E}_0(\mathbf{r})$ is the *free-space* electric field due to current source \mathbf{J}_0 , $\mathbf{E}_s(\mathbf{r})$ the electric field scattered in the *complex surroundings* and $\mathbf{J}_s(\mathbf{r}) = -i\omega\epsilon_0(\epsilon_r - 1)\mathbf{E}(\mathbf{r})$ the induced current in the complex surroundings ($\mathbf{E} = \mathbf{E}_0 + \mathbf{E}_s$). Finally, for a point like electric dipole $\mathbf{J}_0(\mathbf{r}) = -i\omega\mathbf{d}\delta(\mathbf{r} - \mathbf{r}_0)$ it comes

$$\mathbf{d} \cdot \mathbf{E}_s(\mathbf{r}_0) = \epsilon_0 \int d^3\mathbf{r} (\epsilon_r(\mathbf{r}) - 1) \mathbf{E}_0(\mathbf{r}) \cdot \mathbf{E}(\mathbf{r}) \quad (3)$$

$$= \frac{1}{\epsilon_0} \int d^3\mathbf{r} (\epsilon_r(\mathbf{r}) - 1) \mathbf{d} \cdot \mathbf{G}_0(\mathbf{r}_0, \mathbf{r}) \cdot \mathbf{G}(\mathbf{r}, \mathbf{r}_0) \cdot \mathbf{d} \quad (4)$$

where we introduced the free-space electric Green's tensor \mathbf{G}_0 and the Green's tensor associated to the complex environment \mathbf{G} . The electric decay rate modification follows

$$\frac{\Gamma_e}{\Gamma_0} = 1 + \frac{6\pi}{k_0^3|d|^2} \int d^3\mathbf{r} (\epsilon_r(\mathbf{r}) - 1) \text{Im}[f_E(\mathbf{r})] \quad (5)$$

$$f_E(\mathbf{r}) = \mathbf{d} \cdot \mathbf{G}_0(\mathbf{r}_0, \mathbf{r}) \cdot \mathbf{G}(\mathbf{r}, \mathbf{r}_0) \cdot \mathbf{d} \quad (6)$$

Finally, Mignuzzi and coworkers propose to remove material everywhere where $\text{Im}[f_E(\mathbf{r})] < 0$ since it induces decreasing of the decay rate. By iterative procedure they finally obtained *deterministically* complex geometries presenting similar feature as "blackbox" optimization.

In case of a magnetic dipole emission \mathbf{m} , the next term in the expansion of $\int d^3\mathbf{r} \mathbf{J}_0(\mathbf{r})$ in Eq. (2) leads to [56]

$$i\omega\mathbf{m} \cdot \mathbf{B}_s(\mathbf{r}_0) = \int d^3\mathbf{r} \mathbf{J}_s(\mathbf{r}) \cdot \mathbf{E}_0(\mathbf{r}) \quad (7)$$

$$\mathbf{m} \cdot \mathbf{B}_s(\mathbf{r}_0) = -\epsilon_0 \int d^3\mathbf{r} (\epsilon_r(\mathbf{r}) - 1) \mathbf{m} \cdot \mathbf{G}_0^{EH}(\mathbf{r}_0, \mathbf{r}) \cdot \mathbf{G}^{EH}(\mathbf{r}, \mathbf{r}_0) \cdot \mathbf{m} \quad (8)$$

$$= \mu_0 \int d^3\mathbf{r} (\epsilon_r(\mathbf{r}) - 1) \mathbf{m} \cdot \mathbf{G}_0^{HE}(\mathbf{r}_0, \mathbf{r}) \cdot \mathbf{G}^{EH}(\mathbf{r}, \mathbf{r}_0) \cdot \mathbf{m} \quad (9)$$

where the mixed Green's tensor \mathbf{G}^{EH} (resp. \mathbf{G}_0^{EH}) gives the electric field scattered by a magnetic dipole in the complex environment (resp. in free-space). Last line is obtained using $\mathbf{G}_0^{EH} = -(Z_0/\epsilon_0 c)\mathbf{G}_0^{HE} = -(\mu_0/\epsilon_0)\mathbf{G}_0^{HE}$. Finally, The magnetic decay rate modification follows

$$\frac{\Gamma_m}{\Gamma_0} = 1 + \frac{6\pi}{\mu_0 k^3 |m|^2} \text{Im}\{\mathbf{m} \cdot \mathbf{B}_s(\mathbf{r}_d)\} \quad (10)$$

$$= 1 + \frac{6\pi}{k^3 |m|^2} \int d^3\mathbf{r} (\epsilon_r(\mathbf{r}) - 1) \text{Im}[f_H(\mathbf{r})] \quad (11)$$

$$f_H(\mathbf{r}) = \mathbf{m} \cdot \mathbf{G}_0^{HE}(\mathbf{r}_0, \mathbf{r}) \cdot \mathbf{G}^{EH}(\mathbf{r}, \mathbf{r}_0) \cdot \mathbf{m} \quad (12)$$

It is worth noticing that this expression is consistent with the equation used for computing the magnetic decay rate:

$$\int d^3\mathbf{r} (\epsilon_r(\mathbf{r}) - 1) \mathbf{G}_0^{HE}(\mathbf{r}_0, \mathbf{r}) \cdot \mathbf{G}^{EH}(\mathbf{r}, \mathbf{r}_0) = k_0^2 \mathbf{G}_s^{HH}(\mathbf{r}_0, \mathbf{r}_0), \text{ so that} \quad (13)$$

$$\frac{\Gamma_m}{\Gamma_0} = 1 + \frac{6\pi}{k_0 |m|^2} \text{Im}[\mathbf{m} \cdot \mathbf{G}_s^{HH}(\mathbf{r}_0, \mathbf{r}_0) \cdot \mathbf{m}] \quad (14)$$

We plot on figure 6 the sign of the factor $\text{Im}(f)$. Blue areas with $\text{Im}(f) < 0$ reveal where materials has to be removed to enhance the decay rate. Better designing should be obtained from an iterative procedure [38] but we use this approach solely to qualitatively understand the shapes obtained by EO approach. For the sake of clarity and simplicity, we consider the dipolar emission in the glass/Si/air slab since Green's tensors are analytical. For electric dipole parallel to the interfaces, we recover the bowtie aperture antenna configuration [38, 48, 57] with an additional circular grating. For other cases, we observe a circular symmetry, again in agreement with our EO optimization, with notably a core for magnetic Purcell factor optimization but without any core for the electric Purcell factor (not shown). We observe qualitative agreement between

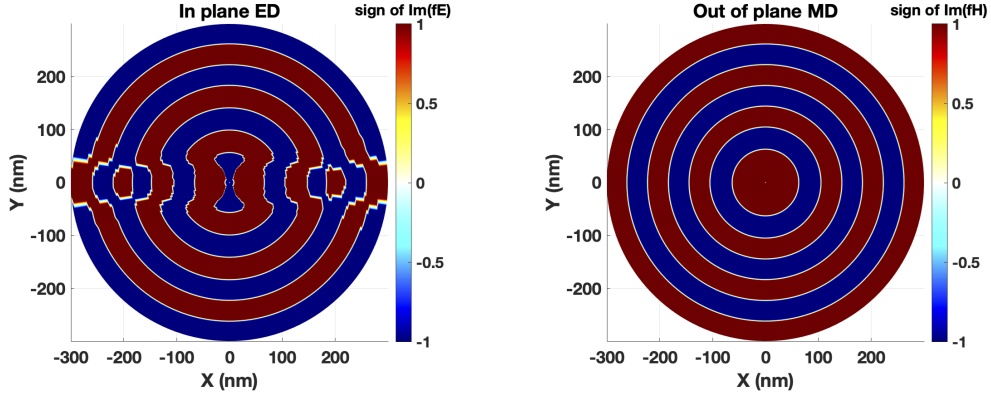


Fig. 6: Sign of the $\text{Im}(f)$ for in plane electric and out of plane magnetic dipoles. The dipole is in the middle of a Si layer (100 nm) sandwiched between a glass substrate and air superstrate.

the shape suggested by removing material where it destructively contributes to the LDOS modification. However, we didn't pursue iterative process to recalculate the constructive or destructive material local contributions to the LDOS at the dipole positions. Therefore, no quantitative agreement could be achieved, notably on the ring periodicity since removing material will strongly modify the effective wavelength in the nanostructured medium. Nevertheless, the approach proposed by Mignuzzi and coworkers clearly reveals the physical origin of the achieved optimized design. In addition, we emphasize that ED and MD emissions are fully analog in free-space. Different reflexions at the interfaces for ED or MD emission is at the origin of the different optimized design.

Reversely, removing material everywhere where $\text{Im}(f) > 0$ (red areas) will minimize the Purcell factor, in agreement with the presented EO simulation of Fig. 3. This also demonstrates the efficiency of the EO geometrical optimization that can be extends safely to other criteria for which no deterministic approach exists.

4 Maximum and minimum achievable magnetic Purcell factor

The obtained optimized structures rely on Si core and a circular grating. Consequently, it presents resonances very sensitive to their shape. Thus, we complete the geometrical optimization by direct finite element method (FEM) simulations to further estimate the maximum achievable magnetic Purcell factor considering this configuration, schemed in Fig. 2. We assume an out of plane MD located at the center of a Gd_2O_3 nanodisk of 50 nm diameter and 100 nm height. It is surrounded by Si cylindrical shell (the core) and a circular gratings constituted of 3 rings. For simplicity, we assume a ring width w_{Si} identical to the Si shell width w_{Shell} surrounding the Gd_2O_3 core. This parameter and the period p of the circular grating has been optimized thanks to a Monte-Carlo simulations of 5000 iterations, see figure 7. We observe a maximum magnetic decay rate enhancement of $\Gamma_m^\perp/\Gamma_0 \simeq 1940$ for a period $p = 125$ nm and a width $w_{\text{Shell}} = w_{\text{Si}} = 49$ nm. This once more demonstrates very high value of the achievable magnetic Purcell factor, largely above the enhancement obtained in bulk high index materials $\Gamma_m^\perp/\Gamma_0 = n^3 \simeq 42$ for Si. Without the circular grating, the Purcell factor is 125 only, demonstrating the role of the grating.

If the Si cylinder shell (the core) is first optimized, without the circular grating, maximum Purcell of 250 is achieved for $w_{\text{Shell}} = 44$ nm. Optimizing the rings width in a second step, we obtain $\Gamma_m^\perp/\Gamma_0 \simeq 1390$ for a period $p = 157$ nm and a ring width of $w_{\text{Si}} = 83$ nm (see figure 8).

Three parameters optimization is needed. However, we observe similar optimized parameters within the experimental fabrication precision so that specific numerical simulations would be performed after

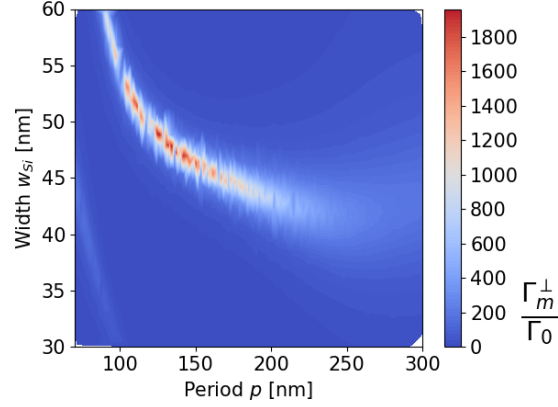


Fig. 7: Results of the Monte-Carlo optimization performed to optimize the width and period dimensions of a bullseye like structure to maximize the decay rate enhancement of a magnetic dipole located at the center of the structure and polarized perpendicularly to the substrate.

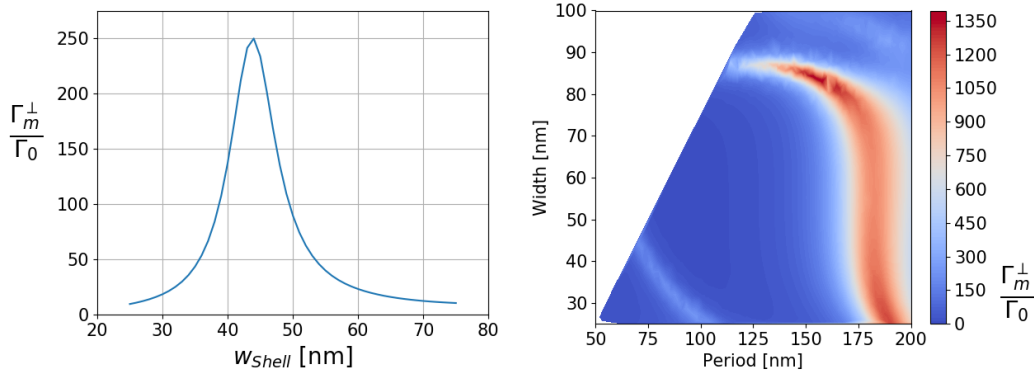


Fig. 8: Left: Magnetic Purcell factor Γ_m^\perp/Γ_0 dependency on the shell's width w_{Shell} (no gratings). Right: Results of the Monte-Carlo with $w_{\text{Shell}} = 44$ nm to optimize the width w_{S_1} and period p dimensions of a bullseye like structure to maximize the decay rate enhancement of a magnetic dipole located at the center of the structure and polarized perpendicularly to the substrate.

experimental characterization.

We have also investigated minimization of the out of plane magnetic Purcell factor performing a Monte-Carlo simulations with 5000 iterations, see Fig. 9. The strongest inhibition is $\Gamma_m^\perp/\Gamma_0 \simeq 1/97$ obtained for a ring period $p = 125$ nm and width $w_{S_1} = 46$ nm. As expected, the geometry is complementary to the optimal design leading to $\Gamma_m^\perp/\Gamma_0 \simeq 1940$.

5 Conclusions

In summary, we have shown that evolutionary optimization process and more precisely differential evolution algorithms are particularly relevant tools for the geometrical optimization of nanophotonics system. Its application to the design of dielectric planar nanoantennas for the enhancement and inhibition of the magnetic and electric Purcell factor has allowed us to retrieve regular and periodic characteristics that are naturally materialized through the evolution of these simulations. Regarding the geometry of the optimized

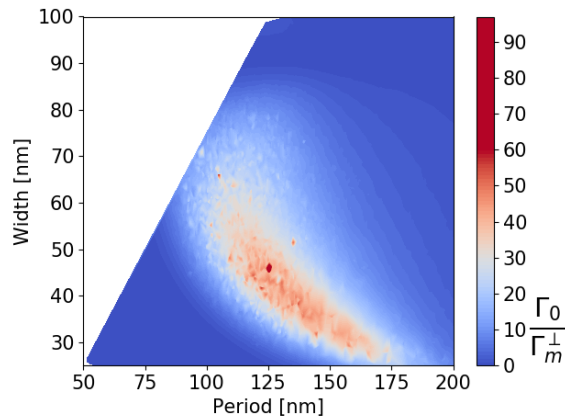


Fig. 9: Results of the Monte-Carlo optimization performed to optimize the width and period dimensions of a bullseye like structure to maximize the decay rate inhibition of a magnetic dipole located at the center of the structure and polarized perpendicularly to the substrate.

nanoantennas shape, bullseye like structure is a common pattern that is arising in the far field region of the dipolar emission either of electric or magnetic nature polarized in or out of the plane. For the near field region, different shapes have been retrieved and analyzed depending on the nature and orientation of the dipole such as dielectric nanodisks or dielectric bowtie nanoantennas. Completed with Monte-Carlo optimizations, we have been able to provide a feasible design of an efficient planar Si nanoantenna deposited on a SiO₂ substrate that leads to a spontaneous decay rate enhancement of the magnetic dipolar transition that occurs at 590 nm in a Gd₂O₃ core doped with Eu³⁺ ions of the order of $\Gamma_m^\perp/\Gamma_0 \simeq 2000$ for an out of plane MD. The concrete realization of such an optimized nanoantenna would lead to a better control of the magnetic light-matter interaction for promising innovative application in quantum technologies or negative index metamaterials.

Funding: This work is supported by the French Investissements d’Avenir program EUR-EIPHI (17-EURE-0002), French National Research Agency (ANR) project HiLight (ANR-19-CE24-0026) and the The European Regional Development Fund FEDER-FSE Bourgogne 2014- 2020, Bourgogne-Franche-Comté.

References

- [1] V. B. Berestetskii, E. M. Lifshits, and L. P. Pitaevskii, in *Quantum Electrodynamics*, 2nd ed., Butterworth-Heinemann, 1982.
- [2] V. Shalaev, Optical negative-index metamaterials, *Nat. Photonics* **1**(1), 41-48, (2007).
- [3] S. Bidault, M. Mivelle, and N. Bonod, Dielectric nanoantennas to manipulate solid-state light emission, *J. Appl. Phys.* **126**(9), 094104, (2019).
- [4] E. M. Purcell, Spontaneous emission probabilities at radio frequencies, *Phys. Rev.* **69**, 674, (1946).
- [5] J. Schuller, E. Barnard, W. Cai, Y. C. Jun, J. S. White, and M. L. Brongersma, Plasmonics for extreme light concentration and manipulation, *Nat. Mater.* **9**(3), 193-204, (2010).
- [6] L. Novotny, and N. van Hulst, Antennas for light, *Nat. Photonics* **5**(2), 83-90, (2011).
- [7] G. Colas des Francs, J. Barthes, A. Bouhelier, J-C. Weeber, A. Dereux, A. Cuche, and C. Girard. Plasmonic purcell factor and coupling efficiency to surface plasmons. implications for addressing and controlling optical nanosources. *Journal of Optics*, 18:094005, 2016.
- [8] A. I. Kuznetsov, A. E. Miroschnichenko, M. L. Brongersma, Y. S. Kivshar, and B. Luk'yanchuk, Optically resonant dielectric nanostructures, *Science*, **354**(6314), 2472, (2016).
- [9] D. G. Baranov, D. A. Zuev, S. I. Lepeshov, O. V. Kotov, A. E. Krasnok, A. B. Evlyukhin, and B. N. Chichkov, All-dielectric nanophotonics: the quest for better materials and fabrication techniques, *Optica* **4**(7), 814-825 (2017).

- [10] P. Wiecha, A. Arbouet, A., C. Girard, A. Lecestre, G. Larrieu, and V. Paillard, Evolutionary multi-objective optimization of colour pixels based on dielectric nanoantennas, *Nat. Nanotechnol.* **12**(2), 163–169 (2017).
- [11] I. Staude, and J. Schilling, Metamaterial-inspired silicon nanophotonics, *Nat. Photonics*, **11**(5), 274–284 (2017).
- [12] T. Wood, M. Naffouti, J. Berthelot, T. David, J.-B. Claude, L. Métayer, A. Delobbe, L. Favre, A. Ronda, I. Berbezier, N. Bonod, and M. Abbarchi, All-Dielectric Color Filters Using SiGe-Based Mie Resonator Arrays, *ACS Photonics*, **4**(4), 873–883, (2017).
- [13] S. Karaveli and R. Zia. Spectral tuning by selective enhancement of electric and magnetic dipole emission. *Physical Review Letters*, 106:193004, 2011.
- [14] L. Aigouy, A. Cazé, P. Gredin, M. Mortier, and R. Carminati. Mapping and quantifying electric and magnetic dipole luminescence at the nanoscale. *Physical Review Letters*, 113(076101), 2014.
- [15] M. Kasperczyk, S. Person, D. Ananias, L. D. Carlos, and L. Novotny, Excitation of magnetic dipole transitions at optical frequencies, *Phys. Rev. Lett.*, **114**(16), 163903, (2015).
- [16] F. T. Rabouw, P. T. Prins, and D. J. Norris. Europium-doped NaYF₄ nanocrystals as probes for the electric and magnetic local density of optical states throughout the visible spectral range. *Nano Letters*, 16:7254–7260, 2016.
- [17] P. Wiecha, C. Majorel, C. Girard, A. Arbouet, B. Masenelli, O. Boisson, A. Lecestre, G. Larrieu, V. Paillard, and A. Cuche. Enhancement of electric and magnetic dipole transition of rare-earth-doped thin films tailored by high-index dielectric nanostructures. *Applied Optics*, 58:1682–1690, 2019.
- [18] S. Bidault, M. Mivelle, and N. Bonod. Dielectric nanoantennas to manipulate solid-state light emission. *Journal of Applied Physics*, 126(094104), 2019.
- [19] R. Chacon, A. Leray, J. Kim, K. Lahlil, S. Mathew, A. Bouhelier, J.-W. Kim, T. Gacoin, and G. Colas des Francs. Measuring the magnetic dipole transition of single nanorods by spectroscopy and fourier microscopy. *Physical Review Applied*, 14:054010, 2020.
- [20] J. A. Dobrowolski, Computer design of optical coatings, *Thin Solid Films*, **163**, 97–110, (1988).
- [21] A. V. Tikhonravov, M. K. Trubetskov, and G. W. DeBell, Application of the needle optimization technique to the design of optical coatings, *Appl. Opt.*, **35**(28), 5493–5508, (1996).
- [22] G.E. Moore, Lithography and the future of Moore’s law, in: *Integrated Circuit Metrology, Inspection, and Process Control IX*, 2439, 2–17 (International Society for Optics and Photonics, May 1995).
- [23] S. Molesky, Z. Lin, A. Y. Piggott, W. Jin, J. Vucković, and A. W. Rodriguez, Inverse design in nanophotonics, *Nat. Photonics*, **12**(11), 659–670, (2018).
- [24] T. Feichtner, O. Selig, M. Kiunke, and B. Hecht, Evolutionary Optimization of Optical Antennas, *Phys. Rev. Lett.*, **109**(12), 127701, (2012).
- [25] T. Feichtner, O. Selig, and B. Hecht, Plasmonic nanoantenna design and fabrication based on evolutionary optimization, *Opt. Express.*, **25**(15), 10828, (2017).
- [26] P. R. Wiecha, A. Arbouet, A. Cuche, V. Paillard, and C. Girard, Decay rate of magnetic dipoles near nonmagnetic nanostructures, *Phys. Rev. B*, **97**(8), 085411, (2018).
- [27] P. R. Wiecha, C. Majorel, C. Girard, A. Cuche, V. Paillard, O. L. Muskens, and A. Arbouet, Design of plasmonic directional antennas via evolutionary optimization, *Opt. Express* **27**(20), 29069–29081, (2019).
- [28] N. Bonod, S. Bidault, G. W. Burr, and M. Mivelle, Evolutionary optimization of all-dielectric magnetic nanoantennas *Adv. Opt. Mater.*, **7**(10), 1900121, (2019).
- [29] A. Y. Piggott, J. Lu, K. G. Lagoudakis, J. Petykiewicz, T. M. Babinec and J. Vucković, Inverse design and demonstration of a compact and broadband on-chip wavelength demultiplexer, *Nat. Photonics*, **9**(6), 374–377, (2015).
- [30] M. M. Elsayy, S. Lanteri, R. Duvigneau, J. A. Fan, and P. Genevet, Numerical optimization methods for metasurfaces, *Laser & Photonics Rev.*, **14**(10), 1900445, (2020).
- [31] M. C. Fu, F. W. Glover, and J. April. Simulation optimization: a review, new developments, and applications, in: *Proceedings of the Winter Simulation Conference, 2005*, 13 (IEEE, December 2005).
- [32] D. E. Goldberg and J. H. Holland, Genetic algorithms and machine learning. *Mach. Learn.*, **3**, 95–99, (1988)
- [33] D. Liu, Y. Tan, E. Khoram, and Z. Yu, Training Deep Neural Networks for the Inverse Design of Nanophotonic Structures, *ACS Photonics*, **5**(4), 1365–1369, (2018).
- [34] K. Yao, R. Unni, and Y. Zheng, Intelligent nanophotonics: merging photonics and artificial intelligence at the nanoscale *Nanophotonics*, **8**(3), 339–366, (2019).
- [35] S. So, T. Badloe, J. Noh, J. Bravo-Abad, and J. Rho, Deep learning enabled inverse design in nanophotonics, *Nanophotonics*, **9**(5), 1041–1057, (2020).
- [36] P. R. Wiecha, A. Arbouet, C. Girard, and O. L. Muskens, Deep learning in nano-photonics: inverse design and beyond, *Photonics Res.*, **9**(5), B182–B200 (2021).
- [37] R. Storn, and K. Price, Differential evolution – a simple and efficient heuristic for global optimization over continuous spaces, *J. Glob. Optim.*, **11**(4), 341–359, (1997).
- [38] S. Mignuzzi, S. Vezzoli, S. A. R. Horsley, W. L. Barnes S. A. Maier, and R. Sapienza, Nanoscale design of the local density of optical states. *Nano Lett.*, **19**(3), 1613–1617, (2019).
- [39] C. Girard, Near fields in nanostructures, *Rep. Prog. Phys.*, **68**(8), 1883, (2005).

- [40] P. R. Wiecha, pyGDM—A python toolkit for full-field electro-dynamical simulations and evolutionary optimization of nanostructures, *Comput. Phys. Commun.* **233**, 167-192, (2018).
- [41] P. R. Wiecha, C. Majorel, A. Arbouet, A. Patoux, Y. Brûlé, G. Colas des Francs and C. Girard, “pyGDM” - new functionalities and major improvements to the python toolkit for nano-optics full-field simulations, *Comput. Phys. Commun.* **270**, 108142, (2022).
- [42] C. Majorel, C. Girard, A. Cuhe, A. Arbouet and P. R. Wiecha, Quantum theory of near-field optical imaging with rare-earth atomic clusters, *J. Opt. Soc. Am. B*, **37**(5), 1474-1484, (2020).
- [43] R. Carminati, A. Cazé, D. Cao, F. Peragut, V. Krachmalnicoff, R. Pierrat and Y. De Wilde, Electromagnetic density of states in complex plasmonic systems, *Surf. Sci. Rep.*, **70**(1), 1-41, (2015).
- [44] S.M Islam, S. Das, S. Ghosh, S. Roy and P. N. Suganthan, An adaptive differential evolution algorithm with novel mutation and crossover strategies for global numerical optimization. *IEEE trans. syst. man cybern., Part B, Cybern.*, **42**(2), 482-500 (2012).
- [45] K. Deb, in *Multi-objective optimization using evolutionary algorithms*, Wiley, 2001.
- [46] M. A. Barry, V. Berthier, B. D. Wilts, M.-C. Cambourieux, P. Bennet, R. Pollès, O. Teytaud, E. Centeno, N. Biais and A. Moreau, Evolutionary algorithms converge towards evolved biological photonic structures, *Sci. Rep.* **10**(1), 12024, (2020).
- [47] B. Gralak, G. Tayeb, and S. Enoch, Morpho butterflies wings color modeled with lamellar grating theory, *Opt. Express*, **9**(11), 567-578, (2001).
- [48] A. Gondarenko, S. Preble, J. Robinson, L. Chen, H. Lipson, and M. Lipson, Spontaneous Emergence of Periodic Patterns in a Biologically Inspired Simulation of Photonic Structures, *Phys. Rev. Lett.*, **96**(14), 143904, (2006).
- [49] F. Biscani and D. Izzo, A parallel global multiobjective framework for optimization: pagmo, *J. Open Source Softw.*, **5**(53), 2338, (2020).
- [50] D. F. Edwards, in *Handbook of Optical Constants of Solids*, ed. E.D. Palik, 547–569, Academic Press, 1997.
- [51] H. Aouani, O. Mahboub, N. Bonod, E. Devaux, E. Popov, H. Rigneault, T. W. Ebbesen, and J. Wenger, Bright Unidirectional Fluorescence Emission of Molecules in a Nanoaperture with Plasmonic Corrugations, *Nano Lett.*, **11**(2), 637-644, (2011).
- [52] M. Born, and E. Wolf, in *Principles of Optics: Electromagnetic Theory of Propagation, Interference and Diffraction of Light*, 7th ed., 85-88, Cambridge University Press, 1999.
- [53] J. Li, N. Verellen, and P. Van Dorpe, Enhancing magnetic dipole emission by a nano-doughnut-shaped silicon disk, *ACS Photonics*, **4**(8), 1893-1898, (2017).
- [54] Y. Yang, B. Zhu, and H. Dai, Strong magnetic field enhancement and magnetic Purcell effect in a dielectric disk-ring composite nanocavity, *J. Opt. Soc. Am. B*, **37**(3), 702-708, (2020).
- [55] T. Feichtner, S. Christiansen, and B. Hecht, Mode Matching for Optical Antennas, *Phys. Rev. Lett.*, **19**(21) 217401, (2017).
- [56] L.D. Landau and E.M. Lifshitz, in *Electrodynamics of Continuous Media*, Pergamon, Oxford, UK, 1960.
- [57] Z. Xie, Y. Lefier, M. Angel Suarez, M. Mivelle, R. Salut, J.-M. Merolla, and T. Grosjean. Doubly resonant photonic antenna for single infrared quantum dot imaging at telecommunication wavelengths. *Nano Lett.*, **17**(4), 2152–2158, (2017).
- [58] A. Cazé, R. Pierrat, and R. Carminati, Spatial coherence in complex photonic and plasmonic systems. *Phys. Rev. Lett.*, **110**(6), 063903, (2013).
- [59] L. Novotny, and B. Hecht, in *Principles of Nano-Optics*, 2nd ed., Cambridge University Press, New York, 2006.

6 Supplementary materials : Detailed EO Results

6.1 Maximizing magnetic or electric Purcell factors

6.1.1 Out of plane magnetic dipole

Figure 10 presents EO optimizations of the out of plane magnetic Purcell factor considering $N = 300, 400, 500$ and 600 Si nanopillars.

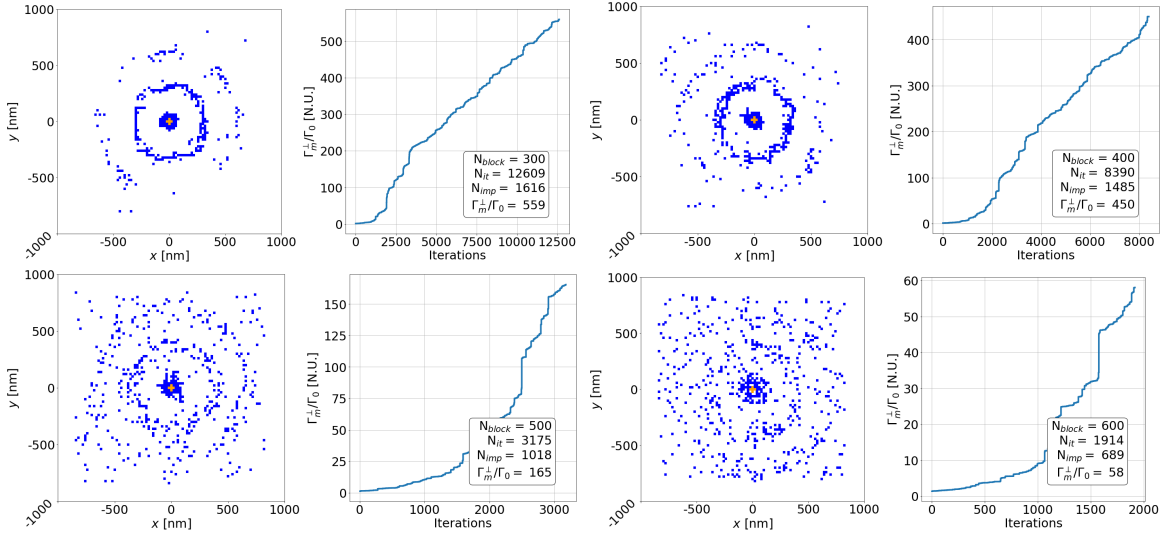


Fig. 10: Left : XY -plane projection of the optimized structure for $N = 300, 400, 500$ and 600 Si nanopillars (orange : fixed core emitter, blue : Si nanopillars), Right : Evolution of the magnetic decay rate enhancement Γ_m^\perp/Γ_0 through the optimization iterations.

We also present in Fig. 11 the superimposition of the four EO optimized structures. This reveals that all the optimizations converge towards a similar configuration, namely a Si core and a circular grating ring.

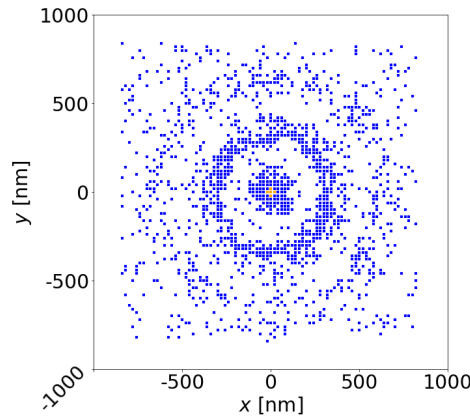


Fig. 11: XY -plane projection of the structure arising from the superposition of the four precedent ones (orange : fixed core emitter, blue : Si nanopillars).

6.2 In plane magnetic dipole

Figure 12 presents optimizations of the in-plane MD for $N = 300, 400, 500$ and 600 Si nanopillars. We obtain an optimized Purcell factor of about $\Gamma_m^{\parallel}/\Gamma_0 \simeq 120$ for a Si core and grating. Once again, the simulation converges towards a regular and periodic structure very similar to the one obtained for the out of plane MD. However, the Si grating seems not fully circular but rather presents two lobes perpendicularly to the dipole orientation. Since dipolar emission is mainly along its axis in the near-field and perpendicular to its axis in the far field, the presence (or not) of matter along the dipole axis in the far-field zone poorly modifies the dipole emission. Again, the superimposition of the optimized structures, shown in Fig. 13, reveals the similarity of the obtained structures.

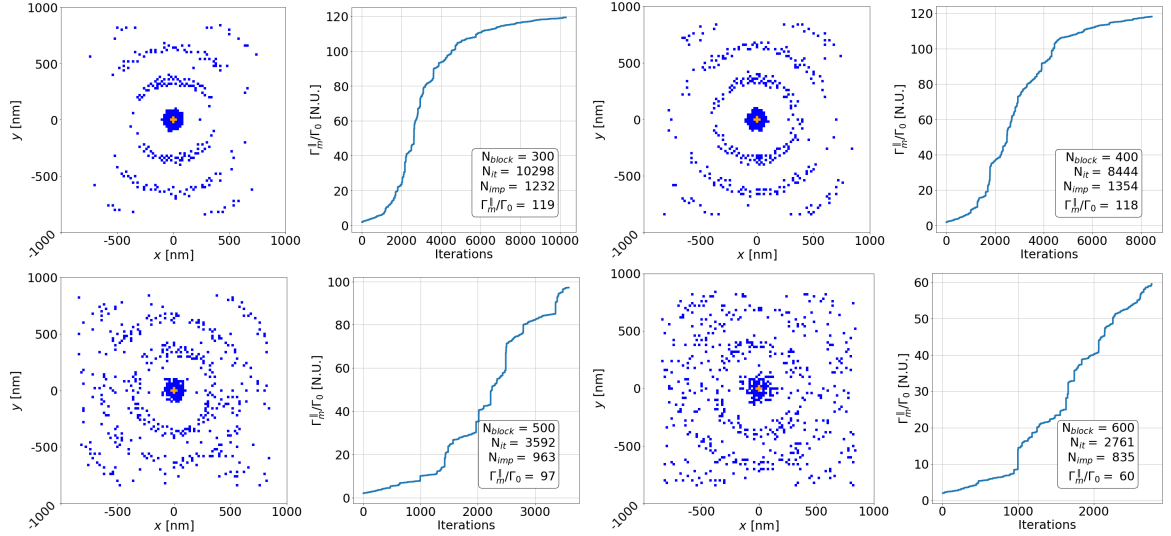


Fig. 12: Left : XY -plane projection of the optimized structure for $N = 300, 400, 500$ and 600 Si nanopillars (orange : fixed core emitter, blue : Si nanopillars), Right : Evolution of the magnetic decay rate enhancement $\Gamma_m^{\parallel}/\Gamma_0$ through the optimization iterations. The MD is along x -axis.

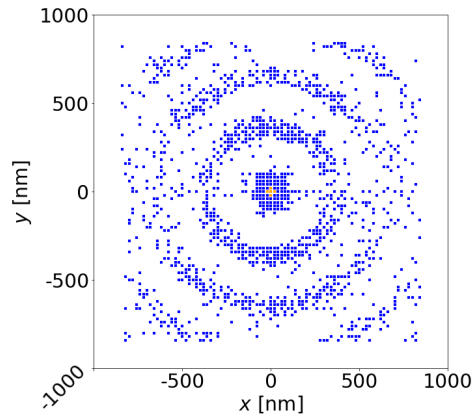


Fig. 13: XY -plane projection of the structure arising from the superposition of the four precedent ones (orange : fixed core emitter, blue : Si nanopillars).

6.2.1 Out of plane electric dipole

Figure 14 presents the results of the exaltation optimization for the electric dipolar emission at λ_e and for a dipole polarized perpendicularly to the substrate for $N = 300, 400, 500$ and 600 Si nanopillars. We observe very low enhancement of the Purcell factor ($\Gamma_e^\perp/\Gamma_0 = 2$), achieved with Si circular grating but without any core. The superimposition of the optimized structures is shown in Fig. 15, facilitating the comparison between the optimized structures, all presenting similar features.

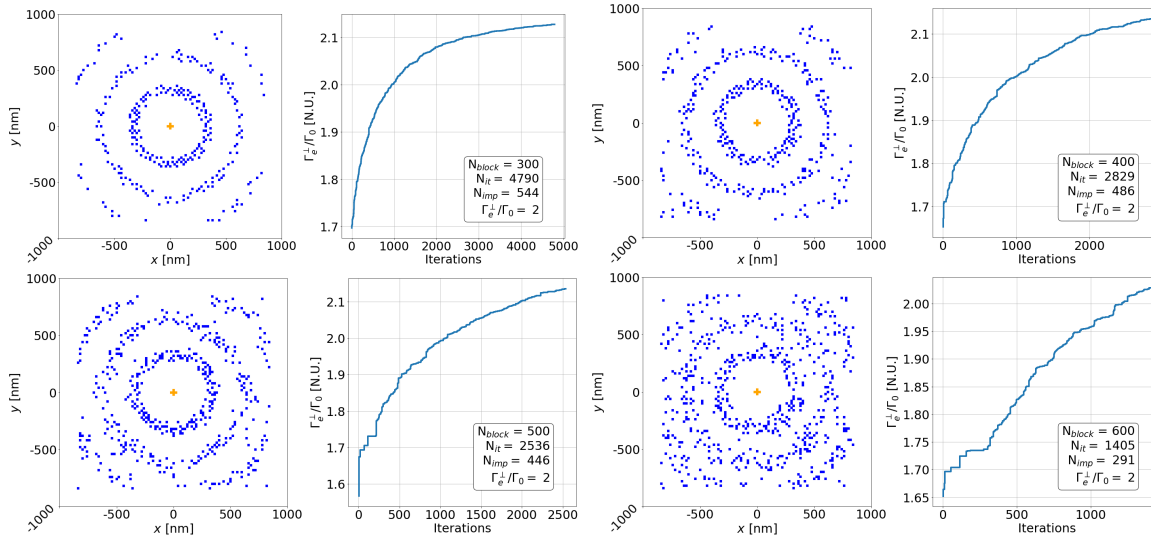


Fig. 14: Left : XY -plane projection of the optimized structure for $N = 300, 400, 500$ and 600 Si nanopillars (orange : fixed core emitter, blue : Si nanopillars), Right : Evolution of the electric decay rate inhibition Γ_e^\perp/Γ_0 through the optimization iterations.

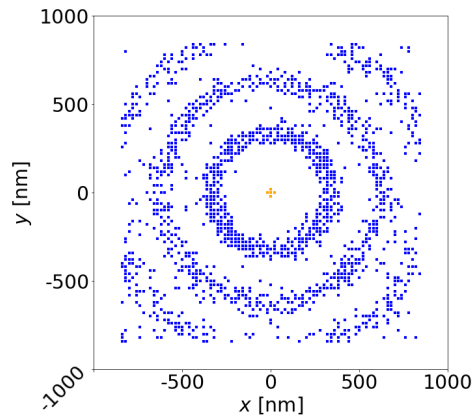


Fig. 15: XY -plane projection of the structure arising from the superposition of the four precedent ones (orange : fixed core emitter, blue : Si nanopillars).

6.2.2 In-plane electric dipole

Figure 16 presents the results of the exaltation optimization for the in plane ED for $N = 300, 400, 500$ and 600 Si nanopillars. This leads to the superimposition presents on Fig. 5 and discuss in the main text.

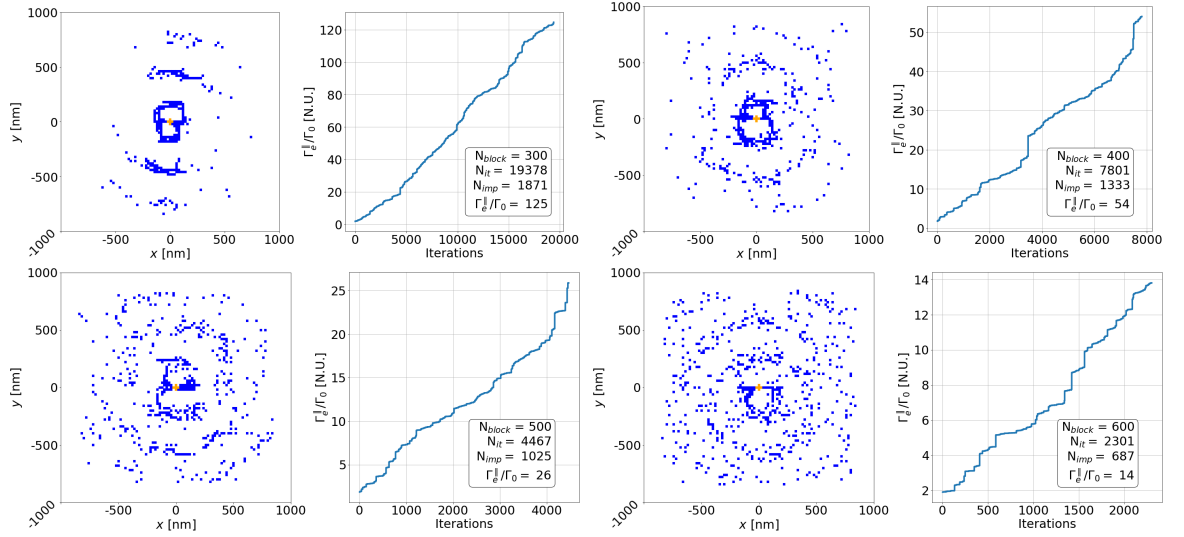


Fig. 16: Left : XY -plane projection of the optimized structure for $N = 300, 400, 500$ and 600 Si nanopillars (orange : fixed core emitter, blue : Si nanopillars), Right : Evolution of the electric decay rate enhancement $\Gamma_e^{\parallel}/\Gamma_0$ through the optimization iterations.